Performance Modeling of Ring Laser Gyro in Inertial Navigation System

Sh. Mohammad-Nejad*, M. Pourmahyabadi* and A. Lajevardizadeh*

Abstract: In this paper, the performance of a Ring Laser Gyro based inertial navigation is investigated. Dynamic and stochastic modeling are applied to gyro simulation and performance evaluation. In the dynamic model, some parameters such as scale factor and environmental sensitivity have been determined, whereas in the stochastic model, the other parameters such as random drift and measurement noise have been computed. The performance of the system is evaluated for several inputs. Also, the parameter variation of output noise as a result of changing the dither characteristics is analyzed.

Keywords: Drift Error, Model Equation, Ring Laser Gyro, Scale Factor Error.

1 Introduction

Ring Laser Gyros (RLG) are effective tools for large scale geodetic surveying at a high level of accuracy. The strapdown RLG inertial systems are widely used for civilian and aircraft navigation [1-4]. They allow rotation of the sensor block with the system and analytical transformation of the output to the coordinate frame of interest; such as frequency difference between two oppositely directed laser beams. This complicated process is affected by internal and external factors, so it is difficult to measure the frequency difference and to convert it to the equivalent angle. On the other hand, test procedures vary widely depending on the facility available and the precise purpose of the test [5-6]. In this case; it is preferred to simulate the behavior of ring laser gyros. Special emphasis is directed at requirements for navigation accuracy, ambient temperature range, vibration environments, and lock in circumvention.

This paper is organized as follows: In the next section, the generic model equation is described. In section 3, it is focused on the gyro modeling and characteristics determination including scale factor error, drift error and their sensitivities. In the next section, the dither influences on Gyro's output, locking effect, scale factor and drift errors are discussed and finally the results are analyzed.

2 Gyro model Equations

All gyros have biases, scale factors, nonlinearities, noise characteristics, and so on. Many of the specification requirements and verification test methods for these parameters; their stabilities; their temperature variation, magnetic, and other sensitivities; the gyro behavior through and across vibration, and other environments; and the gyro lifetime and reliability are independent of the gyro type. The gyro model equation is defined as a series that mathematically relates its output to the components of applied gyro [7-10].

A generic model that applies to many types of sensors is shown in Figure 1. It consists of inertial (including misalignment), environmental, and random (including quantization) contributors. This approach to compartmentalizing gyro model equations is introduced to better organize the various model components. The generic model equation is

$$S_o(\Delta N/\Delta t) = (I + D + E)(1 + 10^{-6}\varepsilon_k)^{-1} \qquad (1)$$

where, S_o is nominal scale factor, $\Delta N/\Delta t$ output pulse rate, I is the inertial input terms, E is the environmentally sensitive terms, D is the drift terms, ε_k is the scale factor error terms (ppm), Ω is the equivalent gyro rate output [11] and

$$
\begin{aligned}
I &= \omega_{IRA} + \omega_{IRA}\sin\theta_N - \omega_{NRA}\sin\theta_L \\
E &= D_T\Delta T + D_{\nabla T}.\nabla T \\
D &= D_F + D_F(t) + D_R + D_Q
\end{aligned}
\qquad (2)
$$

where
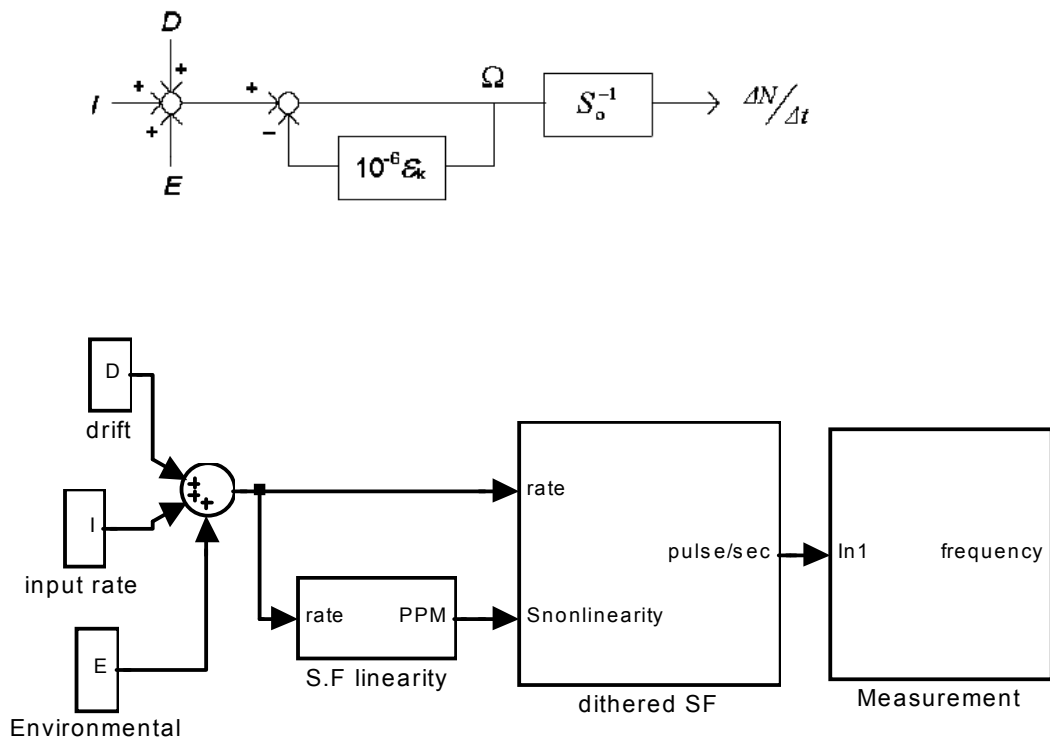
$$D_R = D_{RN} + D_{RB} + D_{RK} + D_{RR} \qquad (3)$$

Fig. 1 Generic model.

In addition, scale factor error is defined by,

$$\varepsilon_K = \varepsilon_T \Delta T + \varepsilon_{\nabla T} . \Delta T + f(\omega_I) \qquad (4)$$

where, ω_{IRA}, ω_{LRA} and ω_{NRA} are the components of the inertial input rate resolved into the gyro reference coordinate frame, θ_L is the misalignment of the IA about the L reference axis (LRA), θ_N is the misalignment of the input axis (IA) about the N reference axis (NRA). D_F is the bias, $D_F(t)$ is the variations of D_F during warm-up period. $D_T.\Delta T$ is the drift rate attributable to a change in temperature ΔT, where D_T is the drift rate temperature sensitivity coefficient. $D_{\nabla T}.\nabla T$ is the drift rate attributable to a temperature gradient ∇T, where $D_{\nabla T}$ is the coefficient vector of the temperature gradient drift rate sensitivity vector. D_{RN} is the random drift rate attributable to angle random walk where N is the coefficient; D_{RB} is the random drift rate attributable to bias instability where B is the coefficient. D_{RK} is the random drift rate attributable to rate random walk where K is the coefficient. D_{RR} is the random drift rate attributable to rate ramp where R is the coefficient. D_Q is the combined effect of the apparent equivalent random drift rate attributable to angle quantization, and the apparent equivalent random drift rate attributable to the anti-lock residual, where Q is the combined coefficient. $\varepsilon_T.\Delta T$ is the scale factor error attributable to a change in temperature ΔT, where ε_T is the scale factor temperature sensitivity coefficient, $\varepsilon_{\nabla T}.\Delta T$ is the scale

factor error attributable to a temperature gradient ∇T, where $\varepsilon_{\nabla T}$ is the coefficient vector of the temperature gradient scale factor sensitivity vector, $f(\omega_I)$ is the scale factor nonlinearity and ω_I is the angular rate about the IA.

3 Modeling

Some of the important applications of modeling occur in simulation studies, performance evaluation, and Kalman filter design. The basic difference between dynamic and stochastic modeling is as follows: in dynamic modeling, given one or more inputs (input vector), and one or more outputs (output vector), it is desired to determine the input/output relationships from both time series. Applications include those where random noise is summing at the output.

In stochastic modeling, on the other hand, there may be no direct access to an input. A model is hypothesized that, as though excited by white noise, has the same output characteristics as the unit under test. Such models are not generally unique, so certain canonical forms are chosen. For example, David Allan of the National Institute of Standards and Technology (NIST) used a power series for the PSD and the corresponding variance analysis in the time domain for the analysis of oscillator stability. This type of variance analysis is discussed in the next part. This is also the objective of the gyro drift analysis.

The general form of the model consists of a mathematical statement of the physical plant equations,

an error model consisting of a perturbation model and environmental sensitivities, a stochastic model describing random drift behavior, and a measurement model consisting of a linear combination of the output states and additive measurement noise. This is related in a generic form of a gyro model equation, consisting of the response to inertial inputs, environmental sensitivities, drift rate, and scale factor error contributors. The shortest way to gain a quantitative understanding of the RLG performance requirements is to review the RLG error sources in relation to the total system error budget [12-13].

3.1   Gyro Errors

Ring laser gyros, ideally, produce pulses representing an exact incremental change in angle. The accumulated gyro pulses, however, are corrupted by both long-term and short-term errors.

Long-term errors result from instability of gyro compensation parameters and include the following terms:

- Bias error
- Scale factor error
- Input axes misalignment error

In the more demanding applications these errors may be further decomposed into temperature sensitive terms. The long -term behavior of these terms influence the error budgets established for each application and are a significant factor in designing the system.

Short-term errors cannot be calibrated and include:

- Dither spillover
- Random walk
- Quantization noise

3.1.1 Drift Errors
3.1.1.1   Random Walk Error

The basic operation of the RLG is to excite and sustain two oppositely directed traveling waves that can oscillate with different magnitudes and frequencies. The fundamental RLG equation is

$$\Delta f = \frac{4A\Omega_{in}}{L\lambda} \qquad (5)$$

Equation 5 shows the RLG frequency difference, commonly called beat frequency (Δf), to be proportional to the product of the geometric area enclosed by the light beams (A) and the angular rate of cavity (Ω_{in}). The beat frequency is also inversely proportional to the product of the vacuum wavelength of the laser (λ) and the optical path of cavity (L). Optical path implies sources of scale factor error. Equation 5 has been obtained with the assumption of no other sources of optical path asymmetry between the two beams other than rotation.

This frequency difference is measured optically via the two light wave interference patterns. As in any mechanical system that sustains two modes of oscillation, problems occur when the two frequencies approach each other. Energy is traded between the two modes and the frequencies tend to lock and become one. This trading of energy or coupling is largely due to the back-scattered radiation from imperfect mirrors. Loss producing mechanisms within the cavity such as outgassing of epoxies also contribute to lock-in. The major technique utilized, at this point in time to circumvent this lock-in has been called "the dither" technique. The technique consists of mechanically rocking the gyro through a stiff dither flexure suspension, which acts as a rotary spring, built into the gyro assembly. It produces a rate about the gyro input axis that causes the gyro to rapidly enter and leave the lock-in zone producing a random drift error [12, 14].

Random walk continues to be the major limitation in reducing the required time of ground gyro compassing prior to system flight. The random-walk error produces an attitude error that builds up as a function of $\sqrt{time}$. It includes four components whose coefficients are determined by Allan variance method:

- Angle random walk (Rate white noise) coefficient
- Bias instability coefficient
- Rate random walk coefficient
- Ramp coefficient

The Allan variance is a reasonable compromise. Simply put, it is a method of representing rms random drift error as a function of averaging time. It is simple to compute, much better than having a single rms drift number to apply to a system error analysis, and relatively simple to interpret and understand. It is not well suited to rigorous analysis, but a reasonable second step in the modeling process. Its most useful application is in the specification and estimation of random drift coefficients in a previously formulated model equation.

To compute these coefficients, a data set from many samples, stored during several periods, is selected. Allan variance method studies the random distributions with additive noise. In this method, the output data affected by additive input noise are predicated. It is supposed that noise distribution is predefined. Then, the noise covariance is estimated by power spectrum density.

The random walk error, D_R is composed of a number of random processes of different origins. Assuming that these processes are independent, the power spectral density (PSD) of D_R can be written as follows:

$$PSD(D_R) = PSD(D_{RN}) + PSD(D_{RB}) + \\ PSD(D_{RK}) + PSD(D_{RR}) \qquad (6)$$

where, $PSD(D_{RN})$ is N^2, $PSD(D_{RB})$ is $B^2/2\pi f$, $PSD(D_{RK})$ is $K^2/(2\pi f)^2$, $PSD(D_{RR})$ is $R^2/(2\pi f)^3$ and f is the

frequency in hertz. The coefficients N, B, K, and R can be evaluated by forming the Allan variance. Therefore,

$$PSD(D_R)=N^2+\frac{B^2}{2\pi f}+\frac{K^2}{(2\pi f)^2}+\frac{R^2}{(2\pi f)^3} \qquad (7)$$

where, R, K, B and N are the random drift coefficients. Bias instability is considered as flicker noise in this equation. Therefore, it is necessary to calculate the temporal average of power spectrum density in Allan variance method. Figure 2 shows a scheme of the drift model [8].
From the test data after the warm-up time, compute the combined anti-lock residual and quantization noise coefficient Q by forming the following Allan variance estimates:

$$\sigma_\Omega^2(nT_O) = S^2[2n^2T_O^2(M-2n)]^{-1}.$$
$$\sum_{m=1}^{M-2n}\left(N_{m+2n}-2N_{m+n}+N_m\right)^2 \qquad (8)$$

for n = 1, 2, 3, ... , $n_{max} \leq (M–1)/2$ and fitting the results to the polynomials in the least squares sense.

$$\sigma_\Omega^2 = \frac{R^2n^2T_O^2}{2}+\frac{K^2nT_O}{3}+B^2\ln(2)\frac{2}{\pi}+\frac{N^2}{nT_O}+\frac{3Q^2}{n^2T_O^2} \qquad (9)$$

where, S is the gyro scale factor, $1/T_o$ is the data sample rate, MT_o is the data record length, Nm is the total output pulses accumulated at time mT_o. The variable n should be selected smaller than the half of M. The achieved variance values will be fitted to a polynomial by using the least mean square.

3.1.1.2 Bias error
Gyro bias error is defined as the difference between the true low-frequency gyro bias (period greater than mission time) and the calibrated gyro bias value loaded in the computer to compensate for this error. As long as this term remains stable and the calibrated value is subtracted from the gyro output, the compensated gyro output will indicate zero rate for the zero rate input condition. Instrument factors affecting gyro bias stability are as follows:
Stability of the mirror's optical axis, and mirror surface.
Outgassing of epoxy materials within the laser cavity.
Precise path length control to correct for changes due to expansion, contraction, and bending of the gyro block material. Equation (5) shows the path length-beat frequency relationship.
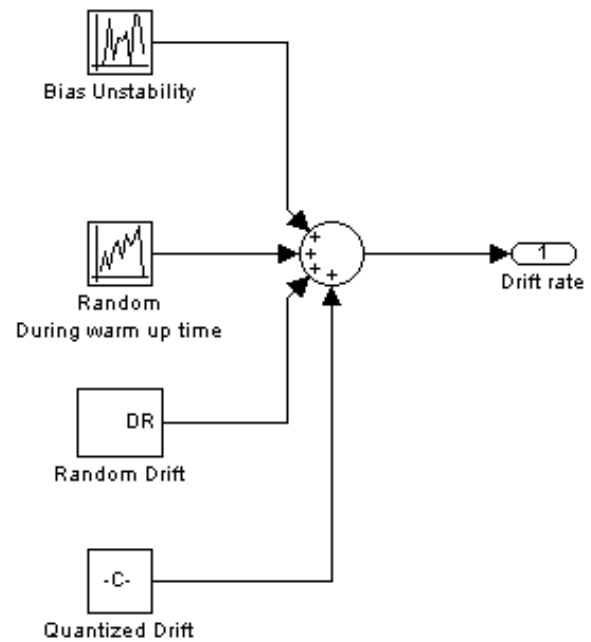Control of the current required to sustain lasing of each beam.

Fig. 2 Drift model scheme [8].

Sufficient control of the dither amplitude to maintain any errors induced by dither to be constant. The forces acting to change dither amplitude are changes in the piezoelectric element's scale factor over temperature; dither change due to external vibration and dither cross coupling.
Because of instability of the fixed bias at the beginning of gyro's turn on, we can fit the resultant data to a time variant function, during the warm up time by using the least mean square method.

3.1.2 Scale Factor Errors
Gyro scale factor is defined as the conversion of gyro output pulse obtained by the fringe motion detector circuits into indicated angle. The basic gyro scale factor is dictated by the inertial angle change to produce one cycle of motion of the beat frequency. It directly depends on laser path length and wavelength. Also it inversely depends on the area of closed path. It is not cataloged exactly because of fabrication error, and hence, it must be measured precisely [11, 14].
Scale factor errors are as follows:

Asymmetry: This is a critical error source that is dramatically reduced using RLG technology over mechanical gyros. The error is defined as the unknown difference between the scale factor for positive rates and that for negative rates is given by,

$$Asymmetry(PPM)=\frac{(S_{c\omega}-S_{cc\omega})}{\frac{1}{2}(S_{c\omega}+S_{cc\omega})}\times 10^6 \qquad (10)$$

Nonlinearity: As mentioned above, the scale factor can be obtained for any rotation rate and numerical scale factor is the mean. Maximum standard deviation indicates to nonlinear error. A simpler means of specifying nonlinearity for lesser accuracy accelerometers is to place limits on composite error as a function of input acceleration, i.e., what is commonly known as an envelope specification. The simplest envelope is to specify that the maximum error over the operating range is a specified percent of the accelerometer full-span output, especially for lesser accuracy accelerometer applications, where it is not intended to compensate for accelerometer nonlinearities that meet the specifications. Acceleration nonlinearities typically arise from structural compliance. Changes in accelerometer temperature that occur under acceleration could manifest themselves as apparent acceleration nonlinearity. The maximum of such effect could be required to be less than the nonlinearity requirement, or the heating could be regarded as a separate temperature sensitivity problem with compensation using temperature sensor measurements if possible.

Repeatability: The standard deviation of the scale factor from the mean of measurements is taken under constant conditions. Other environmental exposures may be substituted or added to the temperature environment specified.

In addition, combinations of various successive environments (e.g., vibration, shock, temperature, remount, power interrupt of specified duration) may be specified. Sufficient time should be allotted to attain thermal equilibrium before making a measurement. Other conditions for repeatability may be specified, such as power-off time with the accelerometer maintained at some fixed temperature.

Stability: It is the variation of scale factor between different operational cycles when the environmental conditions is stabilized. For this purpose, this sensor is set on a rotary disk with a degree of freedom and gyrates with a specific angular velocity (upper than estimated drift/bias velocity). The mean frequency is the ratio of output pulses to sampling interval. Scale factor (Hz/deg-sec or pulse/arc-sec) is obtained by using mean frequency divided by angular velocity. This experiment is repeated in several directions and finally, the mean value is considered as numerical scale factor [2]. In this work, S_o=0.7910929 pulse/arc-sec is obtained without considering the repeatability and stability errors of scale factor.

3.2 Gyro Sensitivities
3.2.1 Drift Sensitivities
Including:
Temperature sensitivity
Temperature gradient sensitivity

The low thermal conductivity of the RLG and its sensitivity to thermal gradients makes heating of the inertial instruments counterproductive.

Magnetic sensitivity: One of the prime mechanisms for RLG magnetic sensitivity is the property of a magnetic field to change the property of light that is not linearly polarized in such a way that a change in gyro drift occurs. All elements of the optical path are optimized to reduce this distortion of the desired linear polarized light.

3.2.2 Scale Factor Sensitivities
Temperature Sensitivity: The gyro scale factor temperature sensitivity resulting from a change in steady-state operating temperature is

$$\frac{S.F_{C_1} - S.F_{C_2}}{C_1 - C_2} \times 10^{-6} \qquad (11)$$

RLG technology has advanced to a point where scale factor thermal stability is good enough to make the requirement for thermal modeling unnecessary to meet thermal scale factor errors of 5 ppm.

Temperature Gradient Sensitivity : It is the change in gyro scale factor resulting from a change in steady-state temperature difference measured across the gyro.

In addition, scale factor is sensitive to the other parameters such as, voltage, temperature rate, acceleration, electromagnetic field vibration, radiance and etc [12, 16].

3.3 Measurement noise
Measurement noise is usually defined as the Allan variance component Q. The purpose of this test is to characterize the noise in the accelerometer output over a wide frequency range. Noise characterization is done by calculating the PSD, Allan variance, and/or rms deviation from the mean output in an IA vertical drift test with or without a trend removed. This noise includes two terms; the first is locking dither residual and the second is quantization noise affected by digitizing output [11, 14]. It will also be obtained by Allan variance method.

4 Results
Ring laser gyros are dithered to prevent a phenomenon known as lock-in. Lock-in is the result of backscattering from the mirrors within the laser cavity causing the two counter-rotating beams to become "mode locked". This phenomenon occurs at low input rates to the gyro. By sinusoidally dithering the gyro a continuous input rate is maintained on the gyro (except for a momentary "turn-around") thus eliminating the lock-in effect. Other methods of biasing the input of an RLG have been developed. However, only the dither method has been

successfully transitioned to production [17]. Therefore, we use a sinusoidal dither with random amplitude which eliminates the locking interval (Figure 3). On the other hand, it increases the angle random walk noise considerably, confined to quantum values by using of the anti-vibrating structures of gyro's frame in the ideal mode. Figure 4 shows the angle random walk noise as a function of cavity length for different laser output power.

As shown in Figure 4, the angle random walk decreases with increasing the cavity length and it increases with increasing the laser output power. In this work, the angle random walk noise is obtained as $0.0023\ ^{\circ}/\sqrt{h}$ which is comparable to available test data in [12, 18].

The dither contributes to nonlinear error of scale factor, related to input variations. Figure 5 shows a plot of the dithered scale factor correction, expressed in parts per million, for dither rates of 100, 200, 300 deg/sec. Both the positive and negative contributions are plotted on the same scale. The negative term has been multiplied by -1, so that it can be scaled relative to the positive term. The value of Ω was chosen so that the maximum values of the two contributions are approximately equal [9]. The result revealed when the rotating rate is equal to the peak dither rate, the error is maximal. The reason

is that the interval locking of sensor is increased to maximum value. Here, the maximum error is 250 ppm.
In addition, the scale factor error is affected by cavity gain and loss (Figure 6). Instability of bias is increased since the mean value of dither rotation is not zero during the sampling period. This parameter is 0.003deg/h.
Furthermore, the offset created by the current difference of laser, discharges in two directions, and increases instability of bias. Figure 7 shows the bias discharge current as a function of total discharge. current. The response related to the sinusoidal input with frequency of 0.1 Hz and amplitude of 10 deg/sec is depicted in Figure 8(a). Also the response related to the fixed input with the peak dither rate of 174 deg/sec, is shown in Figure 8(b).
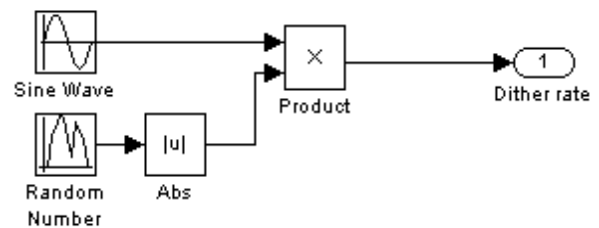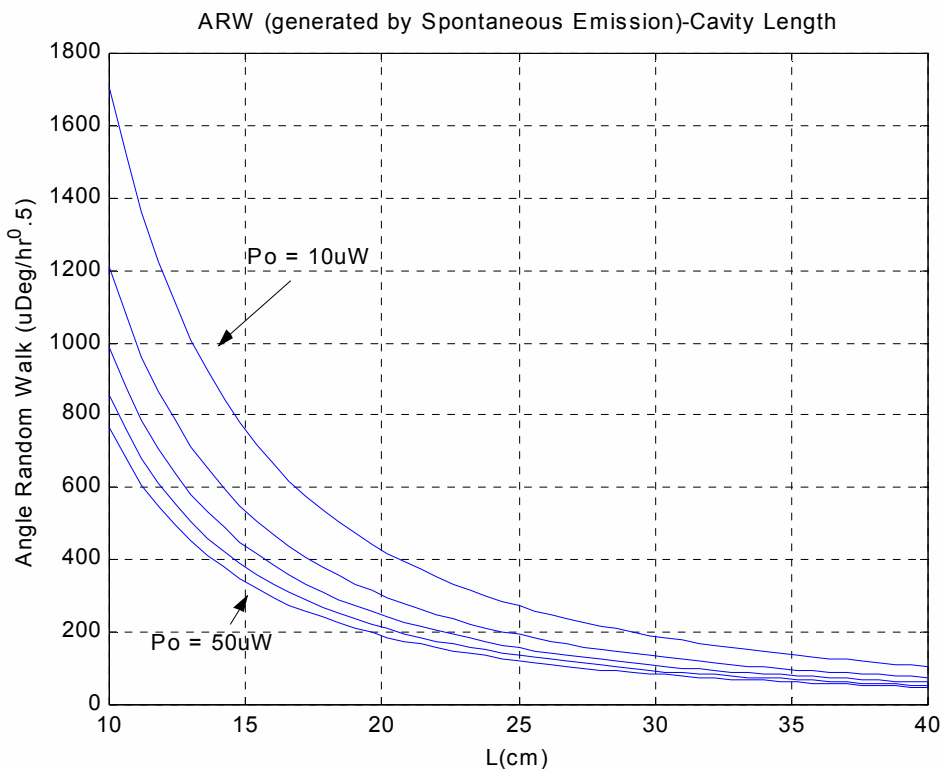

Fig. 3 Dither scheme [9].

Fig. 4 Angle random walk noise versus cavity length.

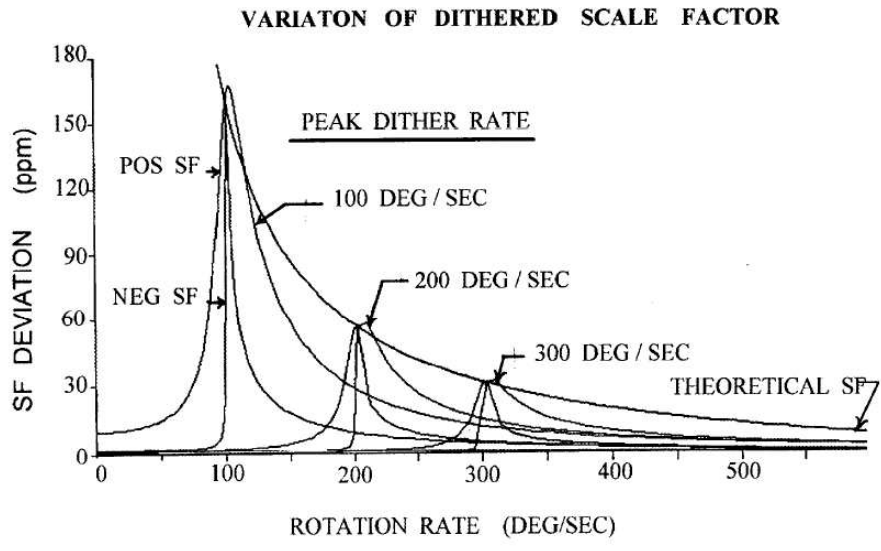## VARIATON OF DITHERED SCALE FACTOR

Fig. 5 These theoretical plots show the scale factor deviation from an arbitrary nominal, for three peak dither rates. The parameters have been adjusted, so as to overlap the positive and negative SF corrections. The negative SF correction shows a smaller width in rotation space, than the positive correction, agreeing with experimental results. The calculated expression, for the peak SF correction when the rotation rate is equal to the dither rate is also shown. Note that it agrees well with the values of the peaks shown on the plot [9].
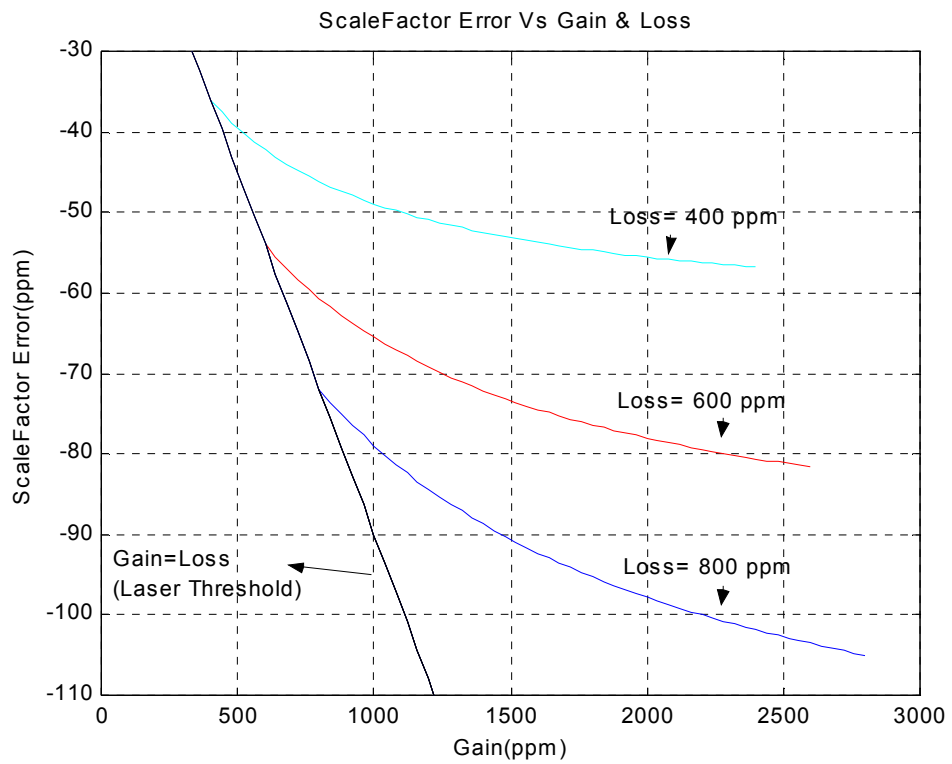

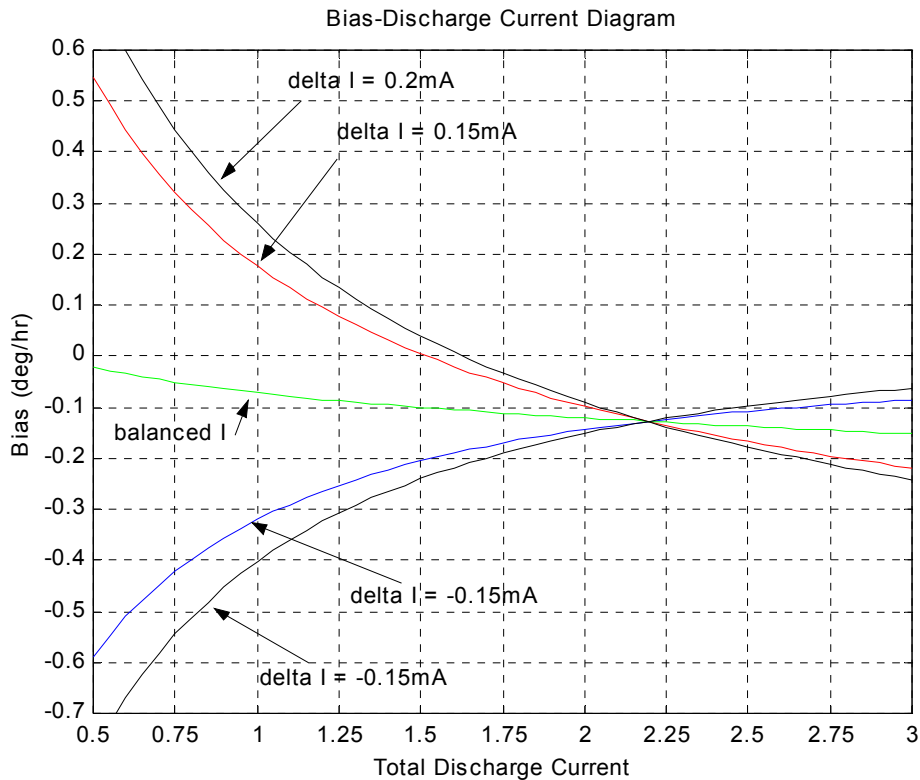**Fig. 6** Scale factor error as a function of gain and loss.

Fig. 7 Bias discharge current versus total discharge current.
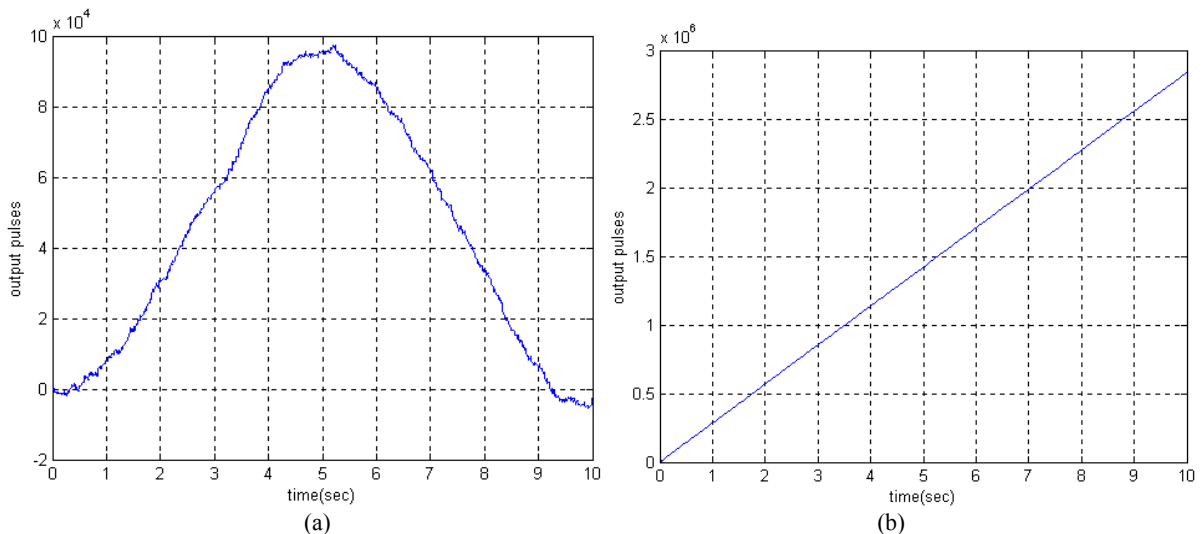

(a)   (b)

Fig. 8 (a) The response related to the sinusoid input with frequency of 0.1 Hz and amplitude of 10deg/sec (b) The response related to the fixed input with the peak amplitude of rotation rate.

5 Conclusion

In this work, the RLG system with respect to its performance has been addressed. It is modeled by using two methods; in the dynamic model, some parameters such as scale factor and environmental sensitivity have been determined, whereas in the stochastic model, the other parameters such as random drift and measurement noise have been computed. The results revealed that the most effective errors found to be the bias instability and

the angle random walk increased by using the dither technique. However these errors will be decreased through the judicious choice of frequency, peak rotation rate and eliminating the temporal mean of rotation rate.

References
[1] KVH Industries, *Overview of compass technology*, Navigation and Special Equipments, 1998, Chapter 3.

[2] Curran, G. L., Engelken, D. J., "Ring laser gyro applications for tactical missiles: the Army TACMS solution," *Position Location and Navigation Symposium, IEEE*, pp. 543–548, March, 1990.

[3] Wright, R. J., Jr., Sponnick, J. V., "A ring laser gyro based navigator for space launch vehicle guidance," *Position Location and Navigation Symposium, IEEE*, pp. 271–279, 1989.

[4] Jekeli, Ch., *Inertial navigation systems with geodetic applications*, Accelerometer and Gyros, Walter de Gruyter, 2000, Chapter 3.

[5] Wong, R. V. C. and Schwarz, K., "Development and field testing of a RLG strapdown inertial survey system," *Position Location and Navigation Symposium*, pp. 480–487, 1998.

[6] King, D., Frin, B. Sc., "Inertial navigation–Forty years of evolution," *Marconi Electronic Systems Ltd.*, Vol. 13, No. 3, 1998.

[7] Gyro and Accelerometer Panel of IEEE, *IEEE standard specification format guide and test procedure for single axis laser gyros*, IEEE, STD 647, 1995.

[8] Gyro and Accelerometer Panel of the IEEE Aerospace and Electronic Systems Society, *IEEE standard specification format guide and test procedure for single axis laser gyros*, IEEE Aerospace and Electronic Systems Society, pp. 1-83, 2006.

[9] Aronowitz, F., *Fundamentals of the Ring Laser Gyro in: Optical Gyros and their Application*, RTO AGARDograph 339, Chapter 3, pp. 1-44, 1998.

[10] Barbour, N., and Schmidt, G., "Inertial sensor technology trends," *The Proceedings of the 1998 IEEE Workshop on Autonomous Underwater Vehicles*, August 1998, Cambridge, MA, pp. 55-62, 1998.

[11] The Missile Technology Control Regime Annex, *Navigation and Special Equipments*, Item. 1, MTCR PUB, 1998.

[12] Kuritsky, M. M., Goldstein, M. S., Greenwood, I. A., Lerman, H., McCarthy, J. E., Shanahan, T., Silver, M., Simpson, J. H., "Inertial Navigation," *Proceedings of the IEEE*, Vol. 71, Issue 10, pp.1156–1176, Oct. 1983.

[13] Gilster, G., "High accuracy performance capabilities of the military standard ring laser gyro inertial navigation unit," *Position Location and Navigation Symposium*, pp. 464–473, 1994.

[14] Mynbaev, D. K., "Errors of an inertial navigation unit caused by ring laser gyros error," *Position Location and Navigation Symposium*, IEEE, pp. 833–38, April 1994.

[15] Lahham, J. I., Wigent, D. J., Coleman, A. L., "Tuned support structure for structure-borne noise reduction of inertial navigator with dithered ring laser gyros (RLG)," *Position Location and Navigation Symposium*, IEEE, pp. 419-428, 2000.

[16] Barbour, N., Schmidt, G., "Inertial sensor technology trends," *Sensors Journal, IEEE*, Vol. 1, Issue 4, pp. 32–339, Dec. 2001.

[17] Dorobantu, R., Gerlach, C., "Investigation of a Navigation-Grade RLG SIMU type INAV-RQH," *IAPG/FESG*, No.16, pp.3-44, 2004.

[18] Oelschlaeger, J. M., "Ring laser gyro inertial measurement systems-honeywell's low cost solution for tactical applications," *Position Location and Navigation Symposium, IEEE*, pp. 528-536, 1999.

Shahram Mohammad-Nejad received his B.Sc. in Electrical Engineering from University of Houston, Houston, USA, in 1981 and M.S. and Ph.D. degrees in Semiconductor Material Growth and Lasers from Shizuoka University, Shizuoka, Japan, in 1990 and 1993, respectively. Professor Mohammad Nejad invented the PdSrS laser for the first time in 1992. He has published over 80 scientific papers and books. Currently, he is the Head of Electrical Engineering Department, Iran University of Science and Technology, Tehran, Iran. Also, he is a scientific committee member of Iranian Conference on Electrical Engineering (ICEE) and also Iranian Conference on Optics & Photonics, member of Institute of Engineering and Technology (IET) and an IET-CEng. His research interests include semiconductor material growth, quantum electronics, semiconductor devices, optoelectronics, electronic devices and lasers.

Maryam Pourmahyabadi received the B.Sc. degree from Shahid Bahonar University, Kerman, Iran, the M.S. degree from Guilan University, Rasht, Iran, both in Electronics Engineering, in 1996 and 1999 respectively. She is currently working toward the Ph.D degree in Electronics Engineering with Iran university of Science and Technology, Tehran, Iran. Her present research interests include optical components/ subsystems for optical fiber communication and fiber sensors.

A. Lajevardizadeh photograph and biography not available at the time of publication.